Mechanics of $(Xe)_N$ atomic chains under STM manipulation

Xavier Bouju*
Laboratoire de Physique Moléculaire, UMR CNRS 6624, Université de Franche-Comté, F-25030 Besançon Cedex, France

Christian Joachim, Christian Girard, and Hao Tang
Centre d'Élaboration des Matériaux et d'Études Structurales, UPR CNRS 8011, 29, rue Jeanne Marvig, Boîte Postale 4347, F-31055 Toulouse Cedex 4, France

(Received 4 July 2000; published 7 February 2001)

The mechanical behavior of short atomic chains under the action of a scanning tunneling microscope (STM) tip is investigated from computerized simulations. The calculation of the constrained atomic positions is performed with a molecular-dynamics approach. The system studied consists of $N(1 \leqslant N \leqslant 5)$ xenon atoms located in the Cu(110)-surface/tetragonal Cu-tip interface. The tunneling current calculation is based on the *elastic scattering quantum chemistry method*. The combination of these two descriptions (electric and mechanical) allows the behavior of the adsorbates to be described precisely. In particular, when working in the operational constant current mode, our numerical scheme behaves as a realistic *virtual STM* that allows an accurate prediction of the intrinsic mechanisms involved in similar experiments. In a first stage, for a single atom we present a diagram summarizing the different possible mechanisms versus the different initial conditions. By adding a second adsorbate, we establish a relation between the adsorbate spacing and the evolution of the tip trajectory [the so-called feedback loop signal (FLS)]. Finally, we present a discussion on the shape of such FLS signals when a linear chain composed of five Xe atoms is laterally pushed by the tip. The extraction of quantitative information on the adsorbate configurations during the manipulation is also addressed.

DOI: 10.1103/PhysRevB.63.085415 PACS number(s): 68.37.Ef, 02.70.Ns, 68.65.−k

I. INTRODUCTION

Individual atoms or molecules adsorbed on surfaces do not behave as classical objects. Their time-dependent average motions $\langle x(t) \rangle$ verify the Ehrenfest mechanical theorem[1] but not the classical dynamic law $md^2\langle x \rangle / dt^2 = -\nabla_{\langle x \rangle} V(\langle x \rangle)$, where V represents the adsorbate-surface interaction potential energy. Formally, a state of translation can always be constructed with the quantized states of the adsorbate mixed with those of the surface. In this manner, we can prepare, at least theoretically, a semiclassical state such that the quantum average position $\langle x(t) \rangle$ follows a quasiclassical trajectory.[2] Nowadays, experimental control of such mechanical behaviors as translational or rotational motions is a real challenge[3,4] because, in practice, such a preparation is not very easy to achieve.[5,6]

The scanning tunneling microscope (STM), generally considered a powerful imaging instrument, can also be viewed as a tool to modify the state of an adsorbate thanks to the external force field generated by its tip apex.[7] During a STM manipulation sequence, the adsorbate appears to behave semiclassically because it seems to follow the tip motion gently.[8] This feature was attributed to the mechanical adsorbate interaction with the STM tip apex, which is nothing but the very end of a macroscopic object. Recently, additonal evidence has reinforced this interpretation.[9,10] Indeed, after a comparison of the experimental feedback-loop signals (FLS's) recorded during a manipulation sequence[9] with those calculated with a pure classical mechanics scheme,[10] no significant differences were observed. A simple molecular mechanics approach satisfactorily reproduces the experimental signals.[10] Nevertheless, in spite of these agreements, the behavior of an adsorbate trapped under a tip apex remains quantum,[11] but the slow motion of the tip associated with the very small bandwidth of the STM feedback does not allow the quantum dynamics to be measured.

In order to explore further how a classical description of the dynamical behavior of an adsorbate during a STM manipulation sequence can be generalized to more complex systems, we have designed a series of numerical experiments. In this paper we investigate the mechanical behavior of short chains of Xe atoms moving under the action of a STM tip. Our study is based on computerized simulations based on the numerical implementation of a virtual STM. This tool, described in a previous paper,[10] is able to reproduce the *feedback loop signals* usually recorded with experimental setups. This information appears to be a genuine signature of semiclassical mechanical effects such as occur at an atomic scale, where they are observed with a STM. Note that a recent numerical study showed manipulation signatures of a single silver atom on a silicon surface at a constant-force mode with an atomic force microscope.[12]

In this paper, emphasis is placed on the change in the *feedback loop signals* as a function of the number of manipulated atoms. In addition, complementary data on the manipulation of a single atom are reported in Sec. III. In particular, we present a diagram of the different possible manipulation mechanisms versus the experimental conditions chosen at the begining of a manipulation sequence.

II. DESCRIPTION OF THE NUMERICAL METHOD

The feedback-loop signals recorded during the lateral manipulation of a $(Xe)_N$ chain can be predicted from a numeri-

cal STM (Ref. 10) able to account for the dynamics of the Xe atoms in the chain. In the four following subsections, we describe the physical basis of this methodology.

A. Main features of the virtual STM code

The implementation of the numerical STM is based on the combination of three different mechanisms.

(i) The tunnel current, calculated by taking into account the chemical specificity of the adsorbates, of the surface and of the probe tip, respectively. In addition to simulating the *constant current mode*, the whole numerical procedure must supply tip-surface distances corresponding to any configuration of the adsorbates inside the junction. The elastic-scattering quantum chemistry (ESQC) technique, already detailed in previous works,[13] is well suited to the realization of these two requirements.

(ii) The adsorption state of the atomic chains described by a molecular-dynamics approach. After each displacement of the tip, the adsorbates are free to move under the interaction field generated by the tip, the surface, and the adsorbates themselves.

(iii) The interdependence between the tunneling current intensity and the position of the atom in the junction. Clearly, the force exerted by the tip modifies the adsorbates' positions, which in turn changes the current in the junction, and thus modifies the tip-surface distance. The tip trajectory that results from this self-consistent process is stabilized by the STM feedback loop system.

A realistic description of the global process needs an accurate representation of the above-mentioned intrinsic mechanisms. In addition, we emphasize the care that must be devoted to the simulation of the STM regulation loop which is the only physical link between the atomic and macroscopic worlds. Consequently, as already mentioned in our previously published papers,[14,15] a standard total-energy calculation of the elements that interact inside a STM junction[16] is not sufficient to compare simulations with experimental results.

B. Computational algorithm

The computational method is illustrated in Figs. 1 and 2, where the schematic STM setup (Fig. 1) and the main stages of the numerical algorithm can be compared (Fig. 2). After setting up the initial tip apex and atom positions, the velocities of the adsorbates, the tunnel current of reference I_{ref}, and the bias voltage V_b, the ESQC-STM program calculates the vertical position of the probe that corresponds to the current condition for the tip-adsorbate configuration. The adsorbates are then left free to relax inside the interface during a predefined time (always chosen much greater than the intrinsic vibrational times inside the junction). This mechanism is treated from a standard Verlet algorithm, in which a phenomenological dissipative term allows the mechanical adsorbate damping to be accounted for. We have adopted a dynamical treatment to find the final adsorbate positions, because the adsorbates evolve along complex pathways that cannot be described with a simple molecular mechanics procedure. Moreover, even if the tip motion is adiabatic, i.e., very slow compared to the atomic motions, the complex geometry of the junction reveals many local minima, and an energy optimization procedure does not allow one to find the correct location of the adsorbates unambiguously.

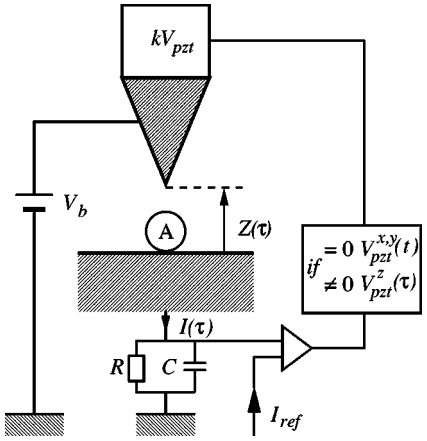

FIG. 1. Schematic electric circuit of a standard STM junction. The circle schematizes the adsorbate, $I(\tau)$ is the tunnel current, and V_{pzt} represents the voltage applied to the piezotranslator. Depending on the output of the comparator element, V_{pzt} acts on the lateral or on the vertical position of the tip. The feedback loop is filtered by a RC circuit.

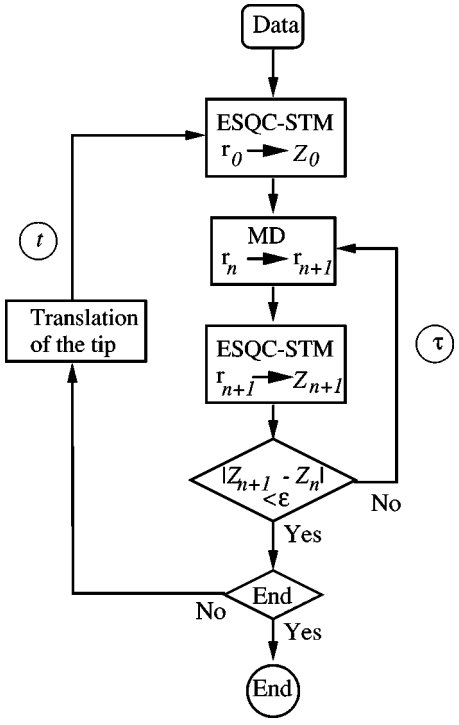

FIG. 2. Schematic algorithm describing the numerical procedure used to simulate the atomic manipulation at constant tunneling current. The three important elements are the stages of molecular dynamics (MD) calculation, of tunneling current evaluation (STM-ESQC), and the autocoherent procedure. Each component of the diagram in Fig. 1 finds correspondence in this algorithm. The scanning time is t, and τ represents the real time of the numerical experiment.

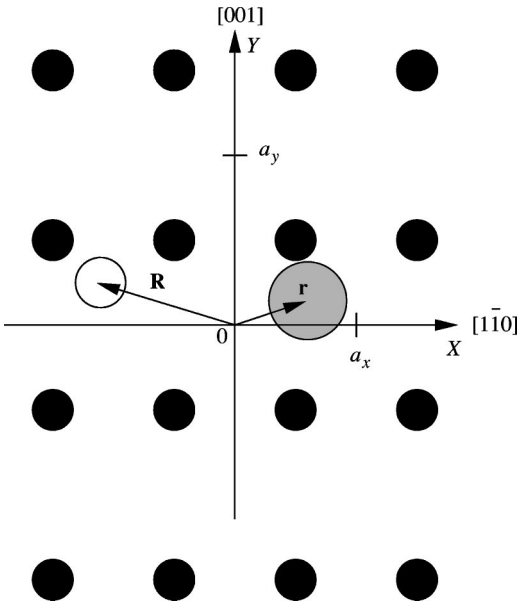

FIG. 3. Partial representation of the STM tip-adsorbate-surface junction. The dark circles symbolize some Cu(110) surface atoms, and the empty circle is the last copper atom ending the Cu[110] tip structure at the position $\mathbf{R}=(X,Y,Z)$. The other tip and surface atoms are not depicted for clarity. The global discrete system consists of 14 and 2890 atoms for the tip apex and the substrate, respectively. The grey circle represents the Xe atom at $\mathbf{r}=(x,y,z)$ in the surface frame. The surface parameters are $a_x=a/\sqrt{2}$ and $a_y=a$, with $a=3.61$ Å.

C. Geometry and interaction potentials

The calculation of the forces acting on the adsorbates is based on four different potential energies describing, respectively, the interactions with the surface, with the atoms of the tip apex, with the tip body, and between the adsorbates themselves. Let us note that for current intensity and the bias voltage used during a manipulation, the effect of the electric field can be neglected.[17]

The system under study is partially represented in Fig. 3. It is composed of 14 copper atoms that constitute the tip apex. This pyramidal cluster is supported by a semi-infinite copper tip body of 20 planes facing a Cu(110) surface. This surface is represented by a discrete slab with ten planes and 289 atoms per plane. The (110) surface parameters are $a_x=2.55$ Å and $a_y=3.61$ Å, which create diffusion channels along the surface atomic rows. This physical configuration represents a model system, relevant to a general discussion of the atomic manipulation mechanisms involving physisorbed particles.

The details of the energetical contributions have been given in previous works for the Xe atom and for molecular systems.[15,18] For a physisorbed atom, the dipolar dispersion energy between the adsorbate and the discrete tip was determined in the framework of the coupled modes by solving a sequence of Dyson equations.[19,15] This method permits us to include many-body contributions associated with van der Waals effects.

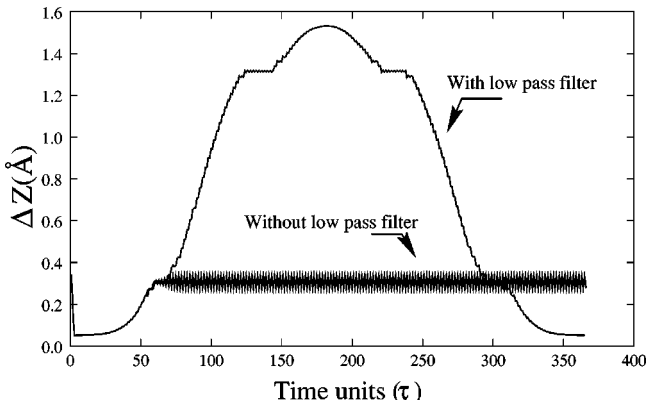

FIG. 4. The imaging process with and without the low-pass filter introduced in the MD stage of the simulation. Without filter, the Z tip position oscillates between two values, and the loop is blocked in a flipflop mechanism.

D. Simulating the experimental feedback loop

The STM feedback loop (Fig. 2) is controlled by a comparator device that acts on the vertical displacement of the tip.[20,21] In our case, the successive vertical positions of the tip are compared to a given threshold. If the variations are less than 0.5 pm, the tip is then displaced laterally; otherwise the self-consistent procedure runs on. The procedure is repeated until the tip reaches its final z position. In order to avoid oscillating situations where the tip and the adsorbates find different configurations with an identical tunnel current, we have introduced a numerical filter in the feedback loop to remove high-frequency oscillations. This numerical filter behaves like the low-pass RC filters used in an STM feedback loop system. In our simulation, it is introduced in the dynamical resolution of the adsorbate motions. Figure 4 illustrates the effect of such a filtering on the STM scanlines of a single xenon atom for $I_{\mathrm{ref}}=1$ nA and $V_b=10$ mV. When the numerical filter is switched off, the tip height oscillates perpetually between two distinct values. In the second case (the bell-shaped curve in Fig. 4), the numerical filter allows the imaging process to be operated. The length of the apparent plateaux reveals the greater or lesser difficulty of the feedback loop to find convergence in particular positions. We recover a corrugation of $\Delta Z\sim 1.5$ Å for the xenon atom, in excellent agreement with the experimental data.[8] In the same manner, the experimental setups also have an intrinsic dumping coming from the piezoceramics response and external low-pass filters acting on the vertical position of the tip.

Our numerical STM relies on three characteristic times. The internal time of the MD (10^{-13} s), the time τ between each MD run (i.e., the duration of the MD stage, typically between 10^{-11} and 10^{-10} s), and the time interval ΔT between two consecutive lateral positions of the tip. This last time duration furnishes a time t proportional to τ: $t=\alpha\tau$. The coefficient α is related to the rapidity of the convergence procedure to find the current threshold.

III. MANIPULATION OF A SINGLE XE ATOM

With a single adsorbate, it is possible to distinguish unambiguously the manipulation mechanism by examining the

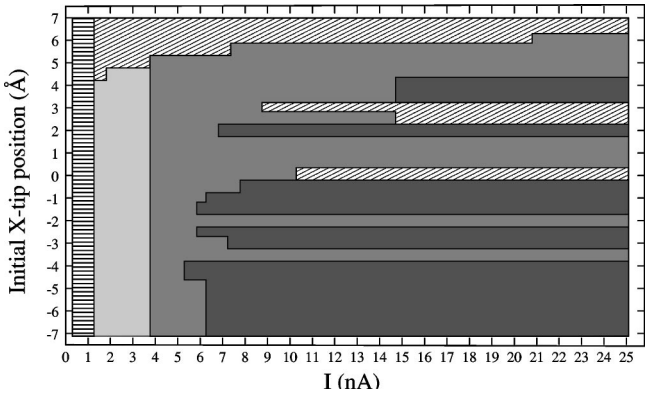

FIG. 5. Diagram showing different modes of STM use according to the initial position of the tip and the tunnel current. The bias voltage is 10 mV. The horizontally dashed zone represents the imaging mode, the light gray zone is the pulling-sliding mode, the medium grey zone accounts for the pulling mode, and the dark grey zones show the pushing process. Finally, no successful manipulation has been observed in the oblique-dashed zones.

shape of the FLS's, as demonstrated experimentally on the Cu/Cu(211),[9] Pb/Cu(211),[9] Ag/Ag(110),[22,23] Cu/Cu(111),[24] CO/Cu(211),[9] Ni/MoS_2,[25] Br/Cu(001),[26] and $C_6H_4I_2$/Cu(111) (Ref. 27) systems. In the Xe/Cu(110) case, we have already demonstrated that our virtual STM was able to simulate manipulations by scanning the tip along the atomic rows of the surface sample.[10] From the feedback loop signals, we can conclude if we are dealing with a pure pulling, a pure pushing, or a pulling-sliding manipulation mode.

A. Analysis of manipulation modes

Figure 5 shows a diagram summarizing the different configurations of a STM used for a scan along the $[1\bar{1}0]$ direction. The tip is initially positioned on the X axis; then the tunnel current is increased by a step of 0.5 nA or 1 nA, until the fixed current threshold is achieved. This constitutes the approach stage. Afterwards, the tip is moved along the $[1\bar{1}0]$ direction to positive X values with the virtual STM procedure. In this way, the different manipulation modes can be determined according to the initial X position of the tip and to the reference current I_{ref}.

(1) For $I_{\mathrm{ref}} \leqslant 1$ nA and whatever the tip position, the virtual STM operates in the imaging mode.

(2) For $1 \leqslant I_{\mathrm{ref}} \leqslant 3.5$ nA, the STM works in the pulling-sliding mode, i.e., in a soft attractive regime.

(3) For $I_{\mathrm{ref}} \geqslant 4$ nA, the Xe atom is manipulated in the pulling or pushing modes, depending on the current value and the initial tip position.

The horizonal stripes appearing for a fixed tip position are a consequence of the approach stage. In fact, when the tip-surface distance is slowly decreased, the adsorbate stays in a limited area during the transient regime before the manipulation. The type of mechanism is determined by the relative location of the tip, i.e., above a hollow site or a bridge site on the surface. For example, with $X=-2$ Å (or $+2$ Å), the Xe atom, placed at the origin of the frame (Fig. 3), is attracted by the probe during the approach and finds a stable position

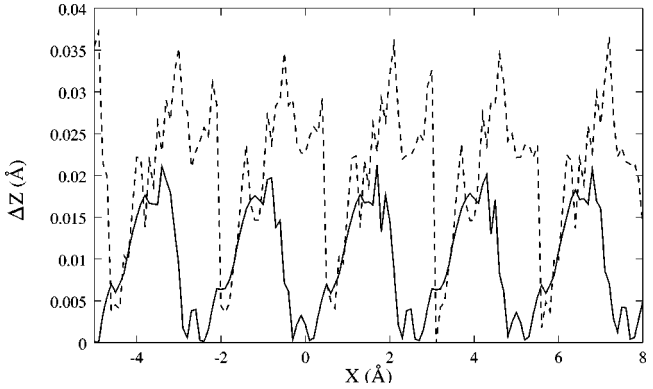

FIG. 6. Feedback-loop signals characteristic of a pushing mode of one adsorbate. The signatures exhibit a quasisinusoidal shape for low tunnel resistances: full line, $R=83\ \mathrm{k}\Omega$; dashed line, $R=125\ \mathrm{k}\Omega$.

in the hollow site at $x \sim -5$ Å ($x \sim 5$ Å). It is then pulled (pushed) when the tip begins to be displaced. Moreover, the asymmetry of the diagram with respect to the $X=0$ position is due to the choice of the tip displacement direction. The two zones with unsuccesful manipulation can be explained by a high repulsive force when the STM finds the current threshold at $X=0$ Å, and by energy accumulated during the final approach at $2.5 \lesssim X \lesssim 3$ Å and a sudden release when the tip begins to be displaced laterally.

The tuning of the tunnel current and the initial position of the tip with respect to the adatom positions allow control of the atomic motion. Recent experiments on the Br/Cu(001) system showed a similar behavior.[26]

B. Some particular features

At the threshold of the imaging mode, we have tried to stabilize a pure sliding mode where the Xe atom would remain exactly trapped under the tip apex during the manipulation, resulting in a pure sinusoidal FLS. Such a mode has not been found, but a quasisymmetrical signal is observed when the probe pushes the adatom with a low tip-surface distance, i.e., at high current. Figure 6 illustrates this kind of signature. This signal reveals the corrugation in the $[1\bar{1}0]$ direction of the surface, enhanced by the presence of a Xe atom close to the tip. At a low tunnel resistance ($R=125\ \mathrm{k}\Omega$ and $R=83\ \mathrm{k}\Omega$), the Xe atom is adsorbed close to a facet of the tip, and is displaced without disturbance from the surface. In this case, the tunnel current mainly originates from the direct tip-surface coupling. The second lateral channel opened by the adsorbate amplifies the apparent surface corrugation.

C. Partial imaging during atomic motion

Within a narrow distance range, we can pass from a pure imaging mode to a situation in which the atom is partially imaged by the tip of the STM.[22,23,26,28–32] In fact, after having located a particular adsorbate on the surface with soft imaging, scanning in a direction perpendicular to the expected manipulation direction can induce a repositioning of

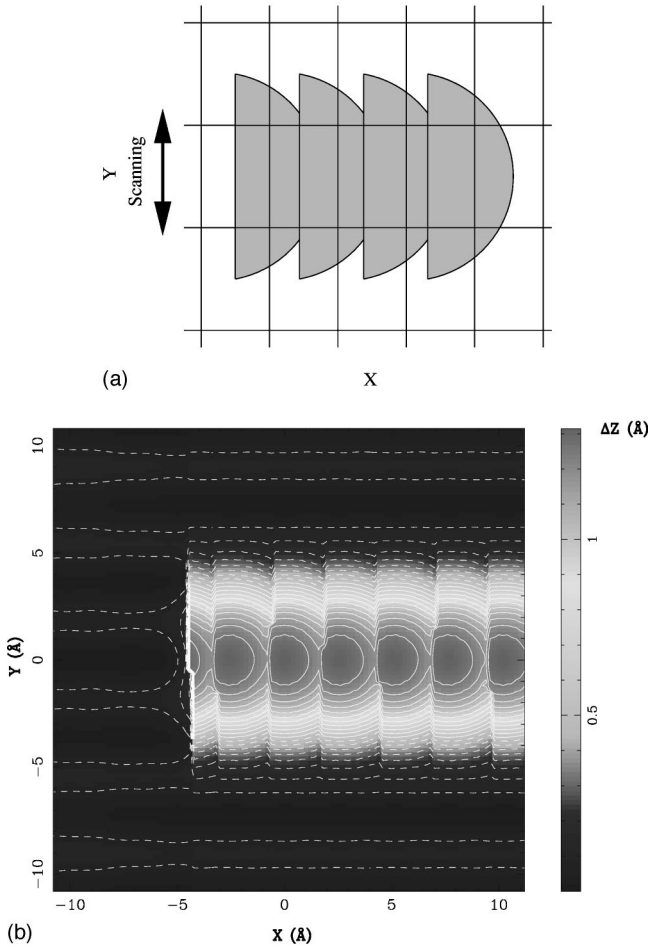

FIG. 7. (a) Representation of the apparent image obtained when the adsorbate is pulled along the *X* direction from the left to the right of the image, and during the scanning of the tip along the *Y* direction. (b) Calculated image of a Xe atom when it is manipulated at $I_{\mathrm{ref}}=1.9$ nA. The initial position of the adsorbate is at the origin of the frame. The grey scale ranges from 0.0 to 1.31 Å, and ΔZ represents the variation of the tip-surface distance.

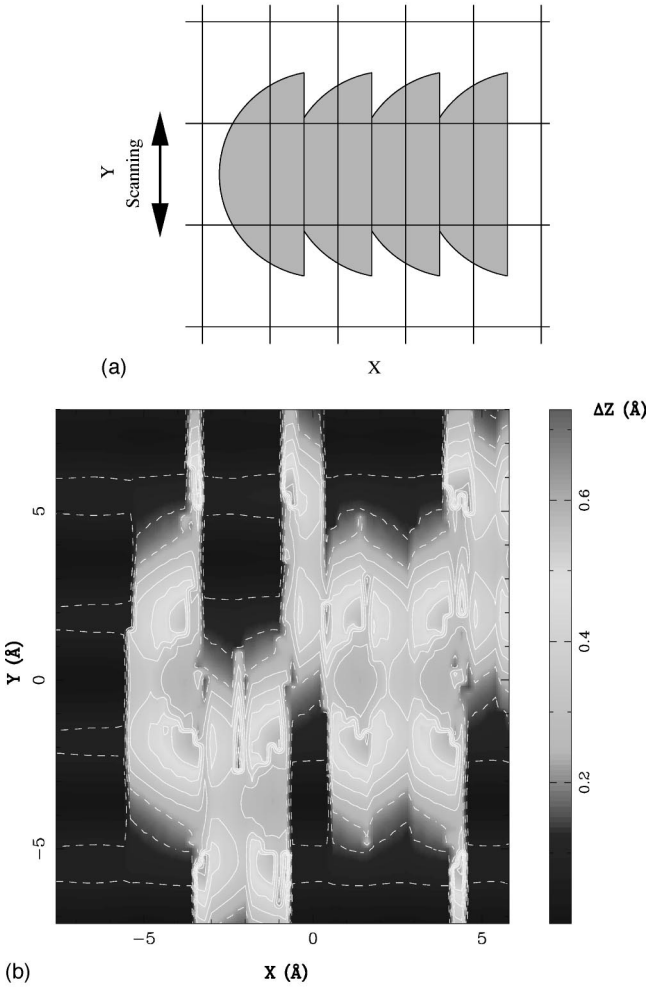

FIG. 8. (a) Idealized representation of a pushing scanning mode manipulation. (b) Atomic manipulation at $I_{\mathrm{ref}}=10.0$ nA during a scanning along the *Y* direction, and from the left to the right of the image. The initial position of the adsorbate is at the origin of the frame. The grey scale ranges from 0.0 to 0.73 Å, and ΔZ represents the variation of the tip-surface distance.

the adspecies by tuning the tunnel current to a favorable value. Li *et al.*[23] studied such a scanning mode manipulation with silver atoms on Ag(110), and their work is at the basis of the following discussion. Figures 7 and 8 show image simulations for a physisorbed system obtained by scanning the probe line by line from the bottom to the top of the image [the tip displacement increment along the rapid scanning direction (*Y*) and the slow one (*X*) is 0.2 Å]. First, when the tip laterally approaches the adsorbate during the scanning at $I_{\mathrm{ref}}=1.9$ nA [Fig. 7(b)], the Xe atom is attracted, and jumps two surface unit cells along the *X* direction ($[1\bar{1}0]$). Then the tip images the top of the Xe atom and pulls it after each scan in the *Y* direction ([001]). We obtain a succession of bumps revealing the manipulation process between hollow sites in a direction perpendicular to the scanning direction. The shape of the image shows a convex half moon oriented along the $[1\bar{1}0]$ direction, as sketched in Fig. 7(a) and as demonstrated experimentally,[23] which determines the manipulation mechanism. By increasing the reference current to 10 nA, we now obtain a mix of pulling and pushing modes. As illustrated in Fig. 8(a), the orientation of the half-moon signal is changed when the tip pushes the adsorbate. Here we see in Fig. 8(b) that some signatures of such a pushing mechanism appear, but they are confused with pulling signatures. In fact, the hopping barrier between two consecutive channels of the (110) surface is low and so the xenon atom is pulled in the *Y* direction and pushed in the *X* direction. These two actions generate a complicated image where two kinds of signatures are present. With the physisorbed system considered here, we have not succeed in reproducing a perfect pushing mode by scanning perpendicularly to the manipulation direction. Moreover, contrary to what is observed experimentally with silver atoms, atomic displacements along the $[1\bar{1}1]$ direction are not found with the system studied here. The diffusion barrier along the [001] direction is smaller than along this diagonal direction,[14] and an exchange mechanism between an adatom and a native surface atom[33–36] is not possible with the Xe/Cu system. These

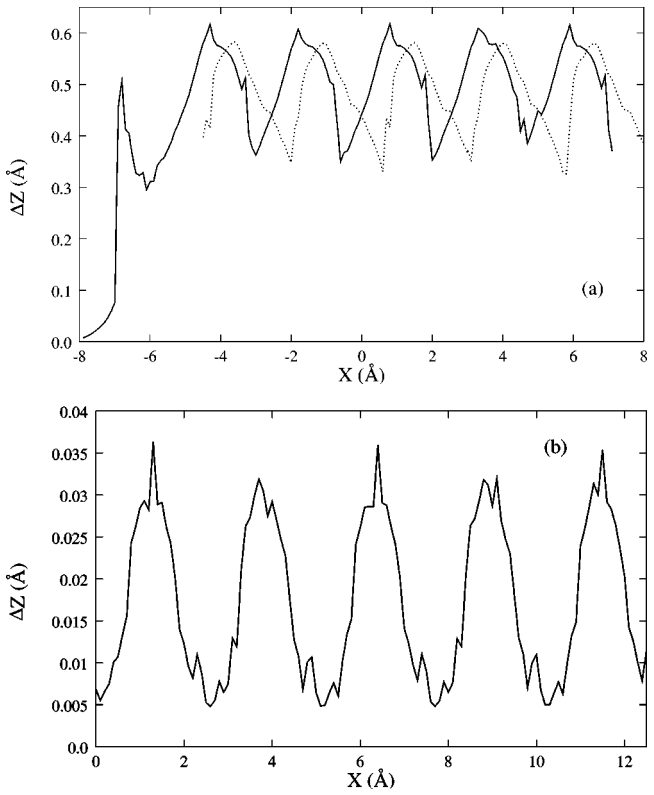

FIG. 9. Feedback-loop signals characteristic of (a) pushing (full line) and pulling (dotted line), and (b) a push-pulling mode of a Xe dimer with $I_{\mathrm{ref}}=7$ nA. The spring constants are $k_1=103.914$ meV Å^2. For the pushing mode, the lateral tip displacement begins at $X=-8$ Å and the two adsorbates are initially at $x=-a_x$ and $x=a_x$ in the $[1\bar{1}0]$ row. For the pulling mode, the lateral tip displacement begins at $X=-4.5$ Å, and the two adsorbates are initially at $x=-4a_x$ and $x=-2a_x$ in the $[1\bar{1}0]$ row. For the push-pulling mode, the lateral tip displacement begins at $X=0$ Å, and the two adsorbates are initially at $x=-a_x$ and $x=a_x$ in the $[1\bar{1}0]$ row.

simulations suggest that, in the case of physisorbed species, the *transverse scanning manipulation mode* described here turns to be less efficient than a direct pulling or pushing of the adsorbate.

IV. MANIPULATION OF TWO XE ATOMS

When manipulating a pair of Xe atoms, the resulting $(Xe)_2$ dimer adds a new degree of freedom to the system. With a weak interaction compared to the metallic $[(Pb)_2$ (Ref. 9)] or chemical $[(CO)_2$ (Refs. 37 and 38)] bondings, this system allows us to test if the internal mechanics shows up on the FLS because of the relatively low frequency of its vibration modes. The purpose of this section is to study whether it is possible to extract this additional dynamical information from the signature. As discussed in Sec. I, due to the macroscopic character of the tip interaction with $(Xe)_2$, these mechanics must be mainly semiclassical.

For a dimer, Bartels *et al.*[9] showed that $(Pb)_2$ on Cu(211) can be pulled with repeated hops, which is revealed by a discontinuous FLS. For $(Xe)_2$ on Cu(110), the FLS's appear without significant sawtooths, and have periods corresponding to the distance between two hollow sites. Nevertheless, the FLS shapes of the pulling and pushing mechanisms described below retain the same tendencies as those observed with one adsorbate, that is, a signature with a succession of slow and rapid slopes.[37]

A. Adatom-adatom potential

The interaction potential between two xenon atoms is described by an accurate pairwise contribution developed by Koutselos *et al.*,[39]

$$V(r)=v_0(Ae^{-ar/\rho}-Be^{-br/\rho})-\left(\frac{C_6}{r^6}+\frac{C_8}{r^8}\right)f(r),$$

with

$$f(r)=\begin{cases} e^{-(1.28R_m/r-1)^2} & \text{if } r\leqslant 1.28R_m \\ 1 & \text{if } r>1.28R_m . \end{cases}$$

The interatomic distance is r, and the coefficients have the following values in atomic units: $C_6=301.00$, $C_8=9965.60$, $v_0=2.911$, $\rho=1.123$, $R_m=8.19$, $A=170.80$, $B=68.51$, $a=1.6203$, and $b=1.5143$. The minimum potential energy is $V_{\mathrm{min}}=-24.397$ meV at a distance $r_0=4.331$ Å. The spring constant is found to be equal to $k_1=(d^2V/dr^2)|r_0=103.914$ meV Å^{-2}.

B. STM signatures

For two adsorbates to be displaced by the STM tip, the FLS's exhibit more regular and continuous structures (Fig. 9). The full line in Fig. 9(a) is the FLS of the following procedure. The tip-surface distance is slightly decreased by increasing the current up to 7 nA. The lateral position of the tip is $X=-8$ Å in the $Y=0$ Å row. The initial positions of the two Xe atoms [labeled $(Xe)_1$ and $(Xe)_2$] are $x_1=-a_x$, $x_2=a_x$, and $y_1=y_2=0$, i.e., they are adsorbed in two hollow sites. When the tip laterally approaches the adsorbates, it attracts the dimer and pushes it along the surface channel. By comparison with a pushing FLS of one Xe atom,[10] we do not observe a sawtooth with abrupt slopes when the adatoms pass over a bridge site during the manipulation. Here the two Xe atoms are trapped by the tip, and the motion of one Xe is constrained by the presence of the second one. The dotted line in Fig. 9(a) describes the pulling process. The two adsorbates are initially placed in hollow sites at $-4a_x$ and $-2a_x$, and the tip begins its approach at $X=-4.5$ Å. The dimer is then pulled during the displacement of the probe. The amplitude of the oscillating signal is about 0.18 Å at the same order of magnitude as in the pushing mode ($\sim$0.25 Å). Finally, we consider the case where the tip is placed just between the two xenon atoms in Fig. 9(b): $X=0$ Å, $x_1=-a_x$, and $x_2=a_x$. Here the tip pulls the first Xe atom and simultaneously pushes the second Xe in the same surface row. Such a push-pulling mechanism exhibits a periodic signal with a low amplitude ($\sim$0.03 Å). This can easily be explained by noting that the tip-surface distance is higher in this case, and that the adsorbates are trapped by a

TABLE I. Different values of the spring constant between two xenon atoms, and the corresponding binding energies.

k (meV Å^{-2})	28.21	77.82	103.91	264.31	403.85	501.31	606.54	806.41	1048.93
V_{min} (meV)	−7.25	−17.92	−24.40	−62.27	−93.11	−113.72	−135.28	−174.53	−395.93

probe with a similar conformation, thus limiting their lateral movements. The sinuslike signature is similar to the signal expected for a pure sliding process of one adsorbate.

C. Modification of the Xe-Xe interaction

To understand how the bonding between the two xenon atoms distorts the FLS, we have *artificially* modified the Xe-Xe potential by changing the spring constant while keeping r_0 constant (see Table I for the modified interaction parameters). In particular, with $C_6 = 10\,001.00$ and $a = 1.389\,615$, the spring constant reaches the value $k_2 = 1048.89$ meV Å^{-2}, with $V_{min} = -395.93$ meV. In this case, the dimer bond is almost rigid. During a pushing manipulation, its mean length only varies by 0.010 Å around a value 4.337 Å. In the pulling mode, it stabilizes around 4.332 Å with a variation of 0.010 Å. With the original spring constant k_1, these values were (4.451 ± 0.154) Å and (4.438 ± 0.151) Å, respectively. The differences in the average values come from the relative interaction with the substrate. The manipulation signatures corresponding to the k_2 value are represented in Fig. 10 for the pushing, pulling, and push-pulling modes.

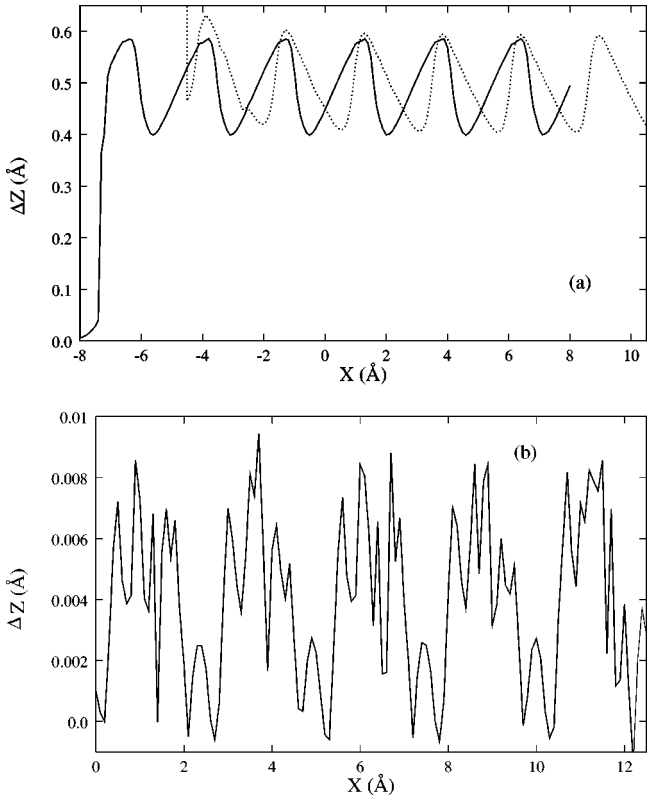

FIG. 10. Same as in Fig. 9, with a spring constant $k_2 = 1048.89$ meV Å^2.

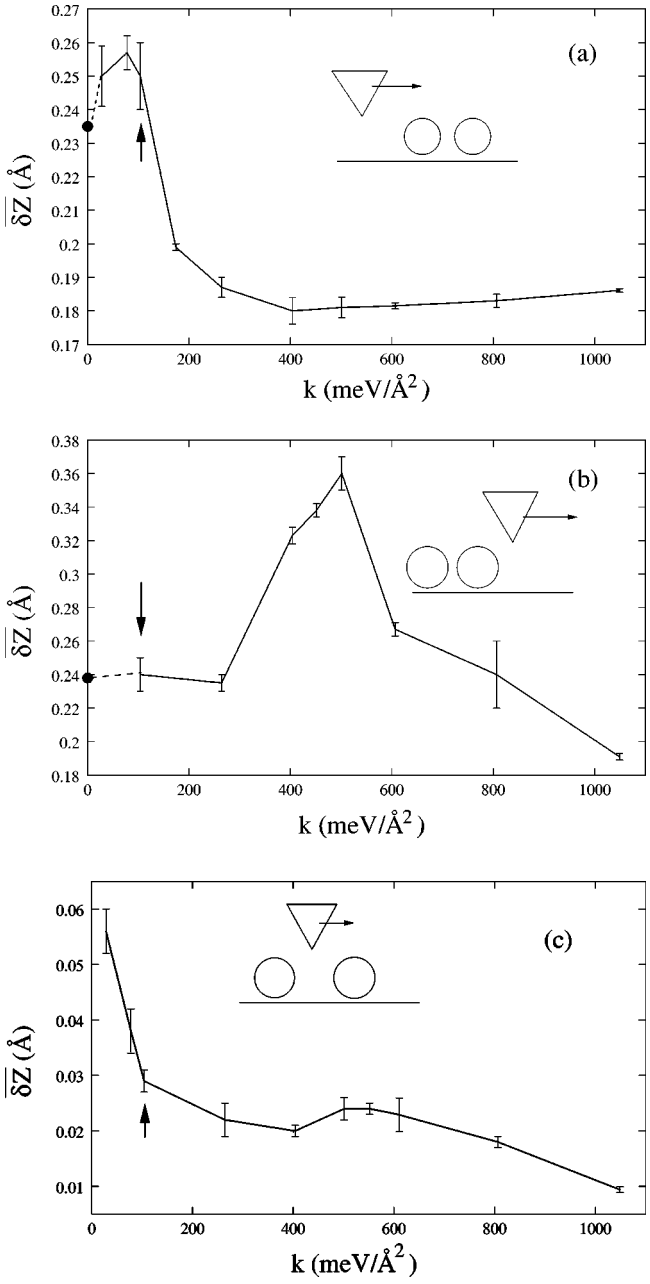

FIG. 11. Variation of $\overline{\delta Z} = \langle \Delta Z_{max} - \Delta Z_{min} \rangle$ for different spring constants of Table I. (a) Pushing, (b) pulling, and (c) push-pulling modes described in the caption of Fig. 9. The black dots correspond to the average value of $\overline{\delta Z}$ obtained with a monomer. The arrows indicate the normal value k_1.

TABLE II. Coordinates $(x_i;z_i)$ of the $(Xe)_i$ atom belonging to the chain with N adsorbates along the $[1\bar{1}0]$ row ($y_i \simeq 0$ Å).

	$(Xe)_1$	$(Xe)_2$	$(Xe)_3$	$(Xe)_4$	$(Xe)_5$
$N=2$	(−4.8461;2.7897)	(−0.2578;2.7895)			
$N=3$	(−4.7795;2.7984)	(0.0006;2.7736)	(4.7862;2.7973)		
$N=5$	(−4.7905;2.7966)	(−0.0413;2.7737)	(5.1053;2.7731)	(10.2515;2.7737)	(14.9993;2.7969)

1. Pulling and pushing modes

For pulling or pushing modes simulated with the k_2 value [solid and dotted lines, respectively, in Fig. 10(a)], the signals now exhibit a continuous, periodic, and asymmetric shape. The orientation of the asymmetry allows one to determine the manipulation mode as for the case of a single Xe atom.[10] The FLS's occurring during a manipulation sequence of a single Xe atom,[10] and those calculated for a rigid dimer as presented in Fig. 10(a), are very similar. The tunnel pathways through the $(Xe)_2$ dimer mainly involve the orbitals of the Xe atom located near the tip. Therefore, the FLS is only sensitive to the movement of the nearest atom. The strong stiffness constant (introduced for the sake of the demonstration) forbids any other movement of the second atom. Then the FLS signal reports the manipulation signal of a Xe atom weighted by the other adatom whose dynamics would not be active. As a direct consequence, the residual irregularities observed on the FLS signal in Fig. 9(a) are due to the movement of the second atom, whose dynamics is not completely governed by the first one. Since the Xe-Xe interatomic distance is quite large, those signature irregularities represent the motion perturbation of the active atom by the other atom. In other words, this contribution does not originate from the tip-apex/Xe-Xe/surface tunnel pathway, contrary to what happens when two adatoms are placed close to the tip, such as in the push-pulling mode or in a vertical configuration,[40,18] and sometimes for admolecules.[42,41] This interpretation will be confirmed by increasing the number of manipulated Xe atoms in the chain (see Sec. V).

2. Push-pulling mode

In the rigid case (stiffness constant k_2), to bring out the influence of the movement of the two Xe atoms from the FLS the manipulation must be performed in the push-pull mode, in which the tip apex is positioned in between the two adsorbates [Fig. 10(b)]. In this case, the FLS is very irregular compared to the FLS of Fig. 9(b), with a smaller amplitude. A Fourier spectral analysis of the FLS reveals a frequency component at about 0.39 $Å^{-1}$, and an important harmonic at 1.56 $Å^{-1}$ that does not occur in the signature of Fig. 9(b) (stiffness constant k_1). Actually, the first spatial frequency (0.39 $Å^{-1}$) corresponds to an intersite distance of 2.56 Å, i.e., the period of the surface corrugation along the atomic rows of the Cu(110) surface. This component is present in both the soft and rigid cases.

To understand the origin of the new harmonic occurring at 1.56 $Å^{-1}$, we have analyzed the trajectory of the dimer during a manipulation sequence in the rigid case. It appears that the rigid dimer is dragged across the surface following a seesawlike behavior. Alternatively, one Xe atom is closer to the tip ($Z=3.0$ Å) than the other ($Z=2.8$ Å). Because of the strong stiffness between the two atoms, when one Xe atom finds a stable position on the surface, the other is forced to be out of registry with respect to the surface. The unexpected harmonic at 1.56 $Å^{-1}$ could originate from this spatial mismatch on the surface. Such an alternate contribution is measurable from the FLS because the in-between position of the tip apex maintains the tunnel pathway through the two xenon atoms. In the nonrigid case, the two atoms refind their respective sites during the manipulation, and this harmonic vanishes. This analysis demonstrates that, by an appropriate choice of the tip-apex position, the FLS is very sensitive to the internal degrees of freedom of the manipulated species.

3. Consequence of the stiffness constant modification

There are additional contributions to the Xe-Xe potential interactions when a $(Xe)_2$ dimer is adsorbed on a surface. For example, the Xe-Xe dispersive interaction is somewhat modified by the small charge transfer toward the surface. This results in a dressed spring constant which is different from that of the isolated dimer. As previously shown after comparison of Figs. 9(a) and 10(a), the FLS amplitude is so sensitive to this spring constant that the amplitude of the phenomenon can be used to evaluate the effective spring constant. In order to clarify this important point, we have calculated the FLS amplitude as a function of the Xe-Xe bond spring constant for the three manipulation modes (Figs. 11). In fact, this amplitude does not vary monotonically as a function of the spring constant value, but exhibits a reso-

TABLE III. In each cell of the table, the left and right numbers represent the interatomic distance (Å) and the interaction energy (meV) between the $(Xe)_i$ and $(Xe)_j$ atoms of the chain with N adsorbates.

	$(Xe)_1$-$(Xe)_2$	$(Xe)_2$-$(Xe)_3$	$(Xe)_3$-$(Xe)_4$	$(Xe)_4$-$(Xe)_5$
$N=2$	4.5883, −22.051			
$N=3$	4.7801, −18.907	4.7856, −18.813		
$N=5$	4.7492, −19.434	5.1466, −13.035	5.1462, −13.042	4.7479, −19.457

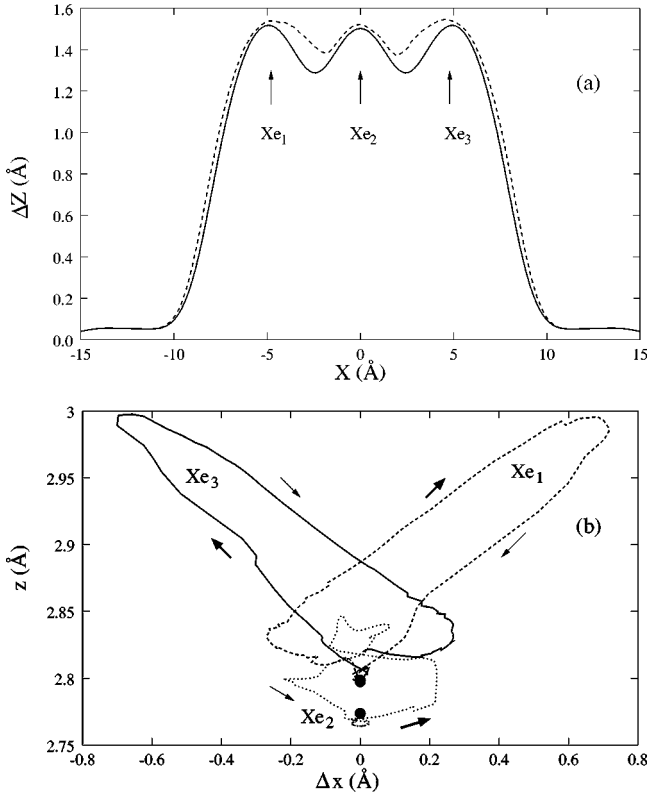

FIG. 12. (a) Scanline of three Xe atom image. The imaging conditions are $I_{\mathrm{ref}}=1$ nA and $V_b=10$ mV. The full line corresponds to calculation with adatoms fixed in their equilibrium sites. The dashed line represents the image of three xenon atoms free to relax. (b) Trajectories in the $(x\text{-}z)$ plane of the three adsorbates during imaging. $\Delta x=x_i(t)-x_i^e$, with x_i^e is the relaxed equilibrium position of $(\mathrm{Xe})_i$ atom along the x axis. The dots indicate the initial position, and the displacement directions of the atoms are shown by the thick arrows followed by the thin ones. The tip scans from the left to the right.

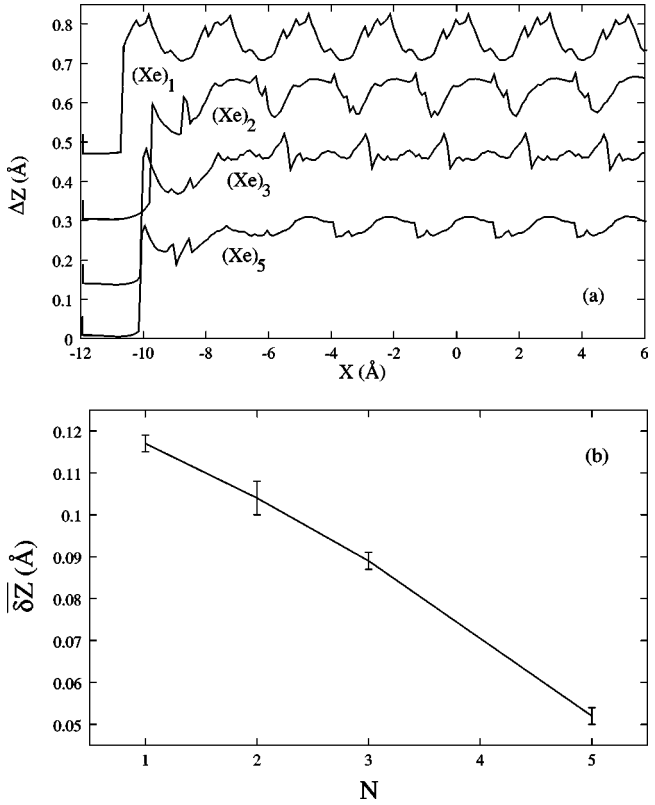

FIG. 13. (a) Different signatures obtained by pushing a $(\mathrm{Xe})_N$ chain with $I_{\mathrm{ref}}=10$ nA. The tip begins its lateral approach at $X=-12$ Å, and the N atoms of a $(\mathrm{Xe})_N$ chain are located at $x_i=(2i-4)a_x$. The successive traces are displaced by a small drift along the y axis for clarity. (b) Variation of $\overline{\delta Z}=\langle \Delta Z_{max}-\Delta Z_{min}\rangle$ for different chain sizes.

nance whose location depends on the manipulation mode. This resonance can be interpreted as a signature of the dimer dynamics excited by the tip apex. In the case of the pushing mode [Fig. 11(a)], the resonance appears for a value of the spring constant smaller than the natural one. A reversal behavior is observed with the pulling mode [Fig. 11(b)]. The maximum is less pronounced in the push-pulling mode [Fig. 11(c)]. Therefore, we can conclude that the pushing mode is more appropriate to detecting low spring constants, while the pulling mode should be used for more rigid dimers. Finally, a comparison of the experimental FLS amplitude with the calculated one should allow an effective Xe-Xe interaction spring constant to be estimated.

V. MANIPULATING $(\mathrm{Xe})_N$ CHAINS

We now consider the manipulation of linear xenon chains $(\mathrm{Xe})_N$. In this section, all simulations have been performed with the natural spring constant k_1 associated with a pair of xenon atoms. As already mentioned in previous sections, a linear xenon chain is not commensurate with the $[1\bar{1}0]$ atomic rows of the Cu(110) surface. More precisely, there is no registry between these two structures because of the incompatibility between their atomic equilibrium distances. As a consequence, because of the weak bonding energy between two consecutive xenon atoms (about 24 meV), the chain will tend to adapt its geometry to the surface geometry. For the same reason, chains of xenon atoms will remain linear,[8] aligned within Cu atomic rows, contrary to what happens with metallic adsorbates, which tend to coalesce.[43] The details of the chain geometry and the interatomic energies are given in Tables II and III as functions of the number of atoms N. Compared to the free dimer interatomic distance, the $(\mathrm{Xe})_N$ chain relaxation is rather important. For example, the dimer remains parallel to the surface, but end effects occur with the trimer and the pentamer. These effects appear with an increase of the distances between the end atoms and the surface, or with a narrowing of the interatomic distances. Similar extremity effects were observed experimentally on the Ni(110) surface with $(\mathrm{Xe})_5$ and $(\mathrm{Xe})_7$ chains.[8] Nevertheless, the value of the interatomic distances measured with the STM must be taken with care, because of the effect of tip adsorbate interaction during the image recording. For example, a STM scan along a trimer is presented in Fig. 12(a), when the chain is frozen in its equilibrium position and when the adsorbates are left free to relax under the influence of the tip. The three independent trajectories, followed by the three

atoms of the trimer during the image acquisition, are given in Fig. 12(b). Relaxation phenomena enlarge the apparent trimer length of about 0.6 Å.

In order to succeed in manipulating longer $(Xe)_N$ chains, the reference current of the virtual STM was chosen to be equal to 10 nA. This current decreases the mean tip-apex surface distance of about 1 Å with respect to the one used to image the trimer (Fig. 12). As shown in Fig. 13(a), we observe (whatever N) a sudden retraction of the tip during the initial lateral approach. This effect is due to the attraction by the tip of the closest atom of the chain, while the other atoms remain located around their equilibrium positions. We have also verified that only the pushing mode efficiently moves a xenon chain with $N>3$. Beyond three atoms, the pulling mode becomes completely ineffective.

In the pushing mode of manipulation, the trajectories of the adsorbates possess a *catch-and-release*-like behavior. Pushing the first atom results in a progressive compression of the chain. The $(Xe)_N$ chain potential energy then increases until the frontal atom overpasses the surface diffusion barrier. Meanwhile, the FLS signal remains mainly sensitive to the physical presence of the first atom. Therefore, the FLS amplitude [Fig. 13(b)] decreases with respect to the chain length, only because the motion of the first atom is damped by the numerous degrees of freedom introduced by the other atoms of the chain. This phenomenon can prevent any extraction of further dynamical information related to the frontal atoms by a simple analysis of the FLS. The FLS appears to be exclusively sensitive to local conformations of the atoms located in the immediate vicinity of the tip.

VI. CONCLUSION

The lateral manipulation of short atomic chains under the action of a STM tip displays a rich panel of interesting features. We have demonstrated that a careful analysis of the FLS allows a real identification of many different manipulation processes (pulling, pushing, sliding, and push pulling). Extensive simulations performed on the dimer case allowed us to conclude that the pushing mode is more appropriate for detecting low spring constant, while the pulling mode should be used for the study of more rigid dimers. In addition, a comparison of the experimental FLS amplitude with the calculated ones should allow an effective atom-atom interaction spring constant to be estimated. In the case of longer chains, the amplitude of the FLS decreases with respect to the number of atoms. This effect can be inferred to be the result of the increasing number of degrees of freedom that occurs when increasing the chain length.

ACKNOWLEDGMENTS

The authors would like to thank Dr. Gerhard Meyer and Dr. Laurent Pizzagalli for fruitful discussions. X.B. acknowledges Professor Jean-Pôl Vigneron for access to the Namur–Scientific Computing Facility of the Université Notre Dame de la Paix (FUNDP).

*Electronic address: xavier.bouju@univ-fcomte.fr

[1] C. Cohen-Tannoudji, B. Diu, and F. Laloë, *Mécanique Quantique* (Hermann, Paris, 1977).
[2] J. Ortigoso, Phys. Rev. A **57**, 4592 (1998).
[3] K. E. Drexler, *Nanosystems: Molecular Machinery, Manufacturing, and Computation* (Wiley Interscience, New York, 1992).
[4] P. W. H. Pinkse, T. Fisher, P. Maunz, and G. Rempe, Nature (London) **404**, 365 (2000).
[5] P. Majumdar and H. S. Sharatchandra, Phys. Rev. A **56**, R3322 (1997).
[6] J. K. Gimzewski, C. Joachim, R. R. Schlitter, V. Langlais, H. Tang, and I. Johannsen, Science **281**, 531 (1998).
[7] J. A. Stroscio and D. M. Eigler, Science **254**, 1319 (1991).
[8] D. M. Eigler and E. K. Schweizer, Nature (London) **344**, 524 (1990).
[9] L. Bartels, G. Meyer, and K.-H. Rieder, Phys. Rev. Lett. **79**, 697 (1997).
[10] X. Bouju, C. Joachim, and Ch. Girard, Phys. Rev. B **59**, R7845 (1999).
[11] I. S. Tilinin, M. A. Van Hove, and M. Salmeron, Phys. Rev. B **57**, 4720 (1998).
[12] L. Pizzagalli and A. Baratoff (unpublished).
[13] Ph. Sautet and C. Joachim, Chem. Phys. Lett. **185**, 23 (1991).
[14] X. Bouju, C. Joachim, Ch. Girard, and Ph. Sautet, Phys. Rev. B **47**, 7454 (1993).
[15] X. Bouju, Ch. Girard, H. Tang, C. Joachim, and L. Pizzagalli, Phys. Rev. B **55**, 16 498 (1997).
[16] U. Kürpick and T. S. Rahman, Phys. Rev. Lett. **83**, 2765 (1999).
[17] X. Bouju, M. Devel, and Ch. Girard, Appl. Phys. A: Mater. Sci. Process. **66**, S749 (1998).
[18] L. Pizzagalli, C. Joachim, X. Bouju, and Ch. Girard, Europhys. Lett. **38**, 97 (1997).
[19] Ch. Girard, A. Dereux, and O. J. F. Martin, Surf. Sci. **295**, 445 (1993).
[20] E. Anguiano, A. I. Oliva, and M. Aguilar, Rev. Sci. Instrum. **69**, 3867 (1998).
[21] M. Aguilar, A. I. Oliva, and E. Anguiano, Europhys. Lett. **46**, 442 (1999).
[22] J. T. Li, R. Berndt, and W.-D. Schneider, Phys. Rev. Lett. **76**, 1888 (1996).
[23] J. T. Li, W.-D. Schneider, and R. Berndt, Appl. Phys. A: Mater. Sci. Process. **66**, S675 (1998).
[24] L. Bartels, G. Meyer, and K.-H. Rieder, Chem. Phys. Lett. **285**, 284 (1998).
[25] J. G. Kushmerick and P. S. Weiss, J. Phys. Chem. B **102**, 10 094 (1998).
[26] T. W. Fishlock, A. Oral, R. G. Egdell, and J. B. Pethica, Nature (London) **404**, 743 (2000).
[27] S. W. Hla, A. Kühnle, L. Bartels, G. Meyer, and K. H. Rieder, Surf. Sci. **454–456**, 1079 (2000).
[28] W. W. Pai, Z. Zhang, J. Zhang, and J. F. Wendelken, Surf. Sci. Lett. **393**, L106 (1997).
[29] B. G. Briner, M. Doering, H.-P. Rust, and A. M. Bradshaw, Phys. Rev. Lett. **78**, 1516 (1997).
[30] M. Böhringer, W.-D. Schneider, and R. Berndt, Surf. Sci. **408**, 72 (1998).
[31] M. Böhringer, W.-D. Schneider, K. Glöber, E. Umbach, and R. Berndt, Surf. Sci. Lett. **78**, L95 (1998).

[32] M. Böhringer, K. Morgenstern, W.-D. Schneider, and R. Berndt, Surf. Sci. **457**, 37 (2000).
[33] C. L. Liu, J. M. Cohen, J. B. Adams, and A. F. Voter, Surf. Sci. **253**, 334 (1992).
[34] L. S. Perkins and A. E. DePristo, Surf. Sci. Lett. **317**, L1152 (1994).
[35] U. Kürpick and T. S. Rahman, Phys. Rev. B **57**, 2482 (1998).
[36] J. J. Schulz, R. Koch, and K. H. Rieder, Phys. Rev. Lett. **84**, 4597 (2000).
[37] G. Meyer (private communication).
[38] L. Bartels, G. Meyer, and K.-H. Rieder, Chem. Phys. Lett. **273**, 371 (1997).
[39] A. D. Koutselos, E. A. Mason, and L. A. Viehland, J. Chem. Phys. **93**, 7125 (1990).
[40] A. Yazdani, D. M. Eigler, and N. D. Lang, Science **272**, 1921 (1996).
[41] P. Sautet and M.-L. Bocquet, Surf. Sci. **304**, L445 (1994).
[42] V. J. Langlais, R. R. Schlittler, H. Tang, A. Gourdon, C. Joachim, and J. K. Gimzewski, Phys. Rev. Lett. **83**, 2809 (1999).
[43] X. Bouju, C. Joachim, and Ch. Girard, Phys. Rev. B **50**, 7893 (1994).